

Supplementary Information: Three-dimensional geometry and topology effects in viscous streaming

Fan Kiat Chan¹, Yashraj Bhosale¹, Tejaswin Parthasarathy¹, and
Mattia Gazzola^{1,2,3†}

¹Mechanical Sciences and Engineering, University of Illinois at Urbana–Champaign, Urbana, IL 61801, USA

²National Center for Supercomputing Applications, University of Illinois at Urbana–Champaign, Urbana, IL 61801, USA

³Carl R. Woese Institute for Genomic Biology, University of Illinois at Urbana–Champaign, Urbana, IL 61801, USA

1. Transitions at infinity

In order to understand the behavior of critical points at infinity, we use the approach of Bhosale *et al.* (2020), where a periodic setup is employed to confine farfield dynamics and bifurcations within repeating unit cells, with the understanding that an infinite domain is recovered as cell boundary approaches infinity. In the following, we present and understand the bifurcations occurring at infinity for both axisymmetric (2D) and non-axisymmetric (3D) cases.

1.1. Fully symmetric setting

We first recall the bifurcations responsible for the single-to-double layer regime transition in the case of the sphere, introduce the overall logic behind the analysis approach, and finally provide precise pointers to previous work, for the interested reader.

From the main text, we observe that the transition introduces saddles that approach the body (as we decrease δ_{AC}/a from the Stokes-like regime) and eventually sit at a distance δ_{DC} away from the body, as observed in the finite thickness layer regime (figure 2 of main text). The appearance of these saddles is mediated by bifurcations occurring at infinity (Bhosale *et al.* 2020). In order to visualize these bifurcations, we can first cast the 3D problem into a 2D problem by virtue of its axisymmetry (i.e. considering a circular cylinder in place of a sphere). Then, by creating repeating units of evenly spaced oscillating cylinders, we form a periodic lattice setup (Bhosale *et al.* 2020). This allows us to confine bifurcations at infinity in between the repeating units and observe them as they unfold. We thus reduced the problem to a 2D setting already thoroughly investigated in Bhosale *et al.* (2020). There, critical background on the equivalence between stream function and autonomous Hamiltonian systems is provided in Section 3.2, and the actual investigation of the single-to-double layer regime is carried out in detail in Section 2.3 of the Supplementary Information. There, we can see how the transition involves a two-step process, where the system first undergo a higher-order hyperbolic reflecting umbilic bifurcation followed by a higher-order elliptic reflecting umbilic bifurcation (Bosschaert & Hanßmann 2013).

† Email address for correspondence: mgazzola@illinois.edu

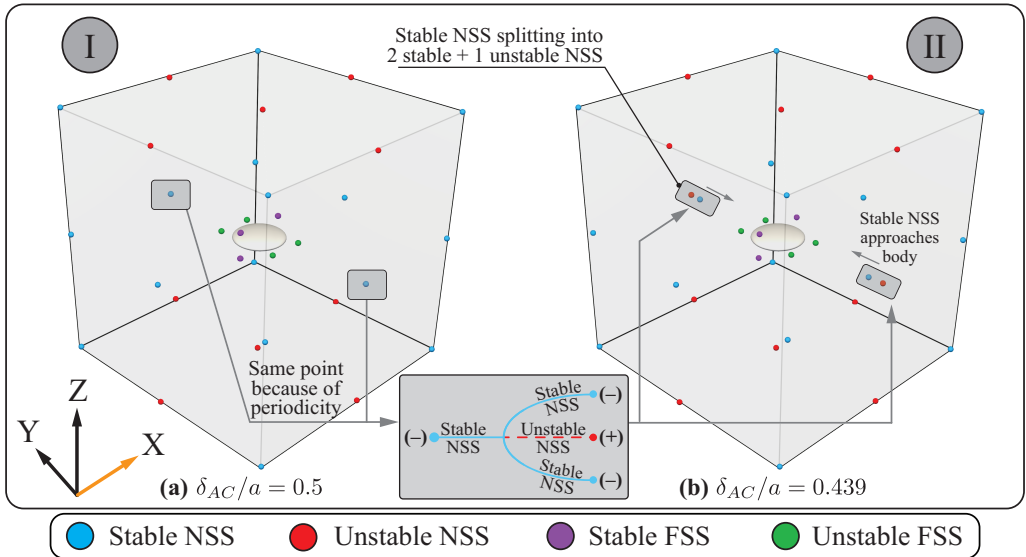


FIGURE 1. Bifurcation at infinity elucidated through periodic setup. Streaming body (spheroid with radii ratio $a_x : a_y : a_z = a : a : 0.25a$) oscillating in a repeating unit bounded by cubic boxes, resulting in critical points defining the flow for (a) Phase I and (b) Phase II. The highlighted stable NSS (blue) undergo supercritical pitchfork bifurcation (inset) to produce two stable (blue) and one unstable (red) NSS, where the new stable NSS eventually approaches the streaming body. Axes orientation are indicated at the bottom-left, and the orange X-axis represents the axis of oscillation. Simulation details: normalized uniform grid spacing $h/a = 0.03$.

1.2. Axisymmetric setting

When investigating the transition from the pocket phase to the finite thickness layer regime for a spheroid oscillating along its axis of symmetry (Section 4.1 of the main text), the disappearance (towards infinity) of the unstable NSS and the appearance (from infinity) of the 2D degenerate saddles (figure 3(c–f) of the main text) can be explained via the same approach above. Again, this process is illustrated in detail in the Supplementary Information of Bhosale *et al.* (2020) in Section 4.4, where elliptic reflecting umbilic bifurcation is identified to be at play.

1.3. Non-axisymmetric setting

We recall here the Phase I \rightarrow II transition from the main text, where we observe a pair of stable FSS approaching the body along the Y-axis as a consequence of supercritical pitchfork bifurcations taking place at infinity. In order to investigate the mechanism responsible for the appearance of these points, we use the same approach above (sections 1.1 and 1.2) and cast the problem in a periodic setup, this time corresponding to a fully 3D repeating lattice. We note that similar mechanisms (either supercritical or subcritical pitchfork bifurcation) can be shown to be at play for other phase transitions involving points approaching from infinity (i.e. Phase III \rightarrow IV and V \rightarrow VI transitions of the main text). Hence, for brevity, we present one such transition here.

Figure 1 illustrates the result of these periodic simulations in Phase I and II, where the streaming body is set to oscillate in a repeating unit bounded by the cubic box. We note that the local flow trajectories are not rendered here to avoid clutter. While we can observe many critical points (stable and unstable NSS) on the boundaries (these critical points are shared between adjacent units), we first draw attention to the stable

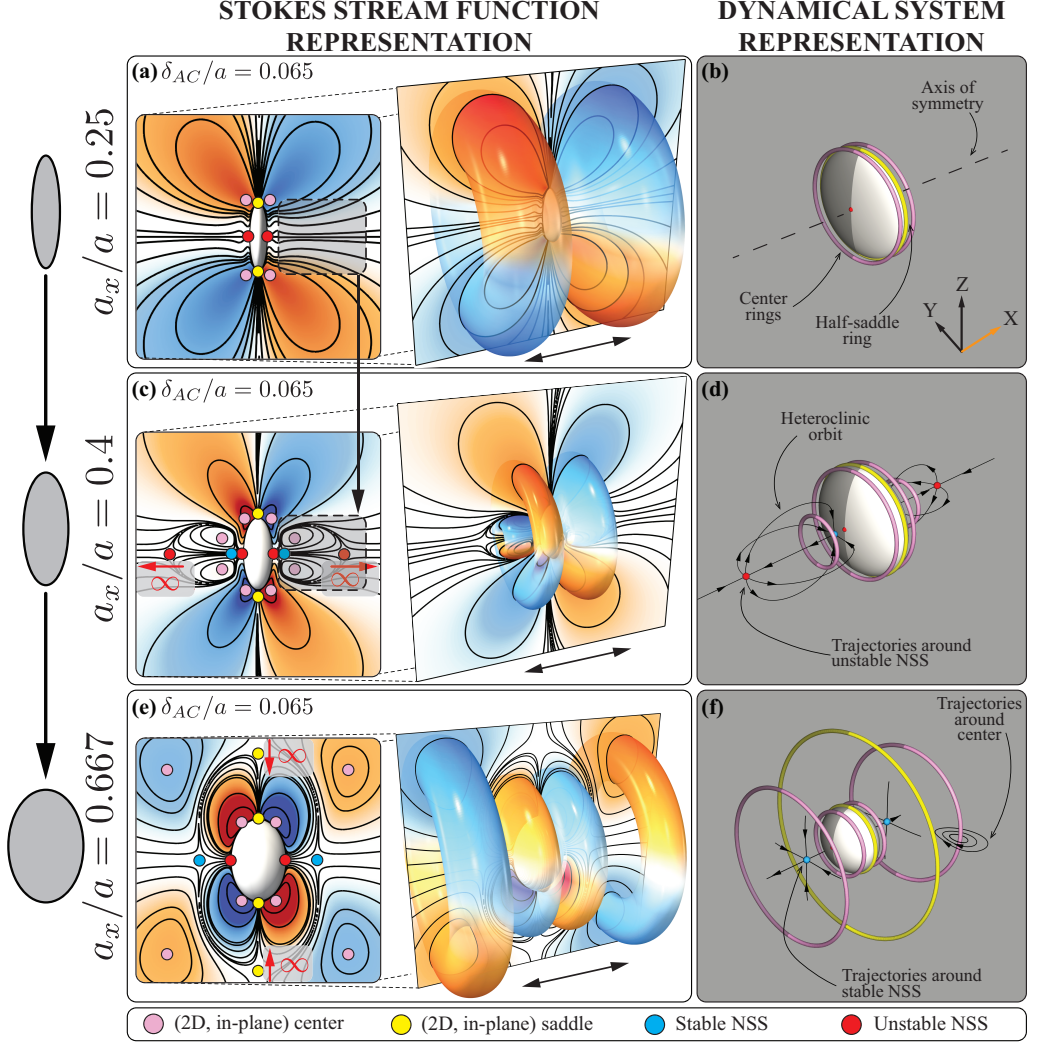


FIGURE 2. Bifurcation through curvature variation in axisymmetric cases. Keeping flow parameter $\delta_{AC}/a = 0.065$ constant while varying the aspect ratio a_x/a of an oscillating spheroid with radii $a_x : a_y : a_z$, where $a_y = a_z = a$, reveals different streaming flow regimes: **(a,b)** Stokes-like regime at $a_x/a = 0.25$; **(c,d)** Flow regime defined by enclosed pockets at $a_x/a = 0.4$; **(e,f)** Finite thickness layer regime at $a_x/a = 0.667$. Simulation details: normalized uniform grid spacing $h/a = 0.03$.

NSS highlighted in figure 1(a). As we decrease δ_{AC}/a from Phase I, we observe that the blue stable NSS undergoes a supercritical pitchfork bifurcation and splits apart into an unstable (red) and two stable (blue) NSS. These new stable NSS (blue) then eventually approach the body as we further decrease δ_{AC}/a , resulting in Phase II, consistent with the observations of the main text.

2. Transition via geometric variation

2.1. Axisymmetric setting

In the main text, we presented three main regimes (Stokes-like, pockets, finite thickness layer) for a spheroid oscillating along its axis of symmetry by varying the flow parameter δ_{AC}/a . Here we show that these regimes are also accessible via geometric variations alone, in keeping with two-dimensional predictions (Bhosale *et al.* 2020). In the following, we oscillate a spheroid of radii a_x and $a_y = a_z = a$ along the X-axis, and vary its aspect ratio $a_x/a < 1$ while keeping flow parameter $\delta_{AC}/a = 0.065$ constant.

We start by considering a flat spheroid of aspect ratio $a_x/a = 0.25$, where we encounter the Stokes-like regime characterized by the single-layer structure as shown in figure 2(a,b). Upon increasing a_x/a to a critical value, we observe the emergence of the neatly enclosed pockets of fluid on both sides of the body (figure 2(c,d)), consistent with the observation in figure 3 of the main text. A further increase in a_x/a brings the flow to the finite thickness layer regime, where the characteristic double-layer recirculating regions can be seen (figure 2(e,f)). Finally, we note that the transitions from single- to double-layer regime achieved via geometric variations here undergo the same bifurcations as those observed by varying flow parameter δ_{AC}/a (figure 3 of main text).

2.2. Non-axisymmetric setting

In the main text, we discovered seven distinct phases between Stokes-like and finite thickness layer regimes for an oscillating spheroid in a non-axisymmetric setting. These phases are also accessible via geometric variation alone, consistent with the above discussion. Indeed, the transitions induced by geometric variations are mediated by the same mechanisms as those observed in figure 4 of the main text. Here, for brevity, we demonstrate two such transitions by changing the aspect ratio a_z/a of a spheroid with radii $a_x = a_y = a$ and a_z oscillating along the X-axis, while keeping δ_{AC}/a constant.

2.2.1. Phase II \rightarrow III

Here we demonstrate the Phase II \rightarrow III transition at constant $\delta_{AC}/a = 0.316$. We start by considering a spheroid of aspect ratio $a_z/a = 0.5$ as shown in figure 3(a), where we encounter a flow representative of Phase II. Upon decreasing a_z/a to a critical value, we observe that the stable NSS (blue) on both sides of the body split into an unstable NSS (red) and a pair of stable FSS (purple) as shown in figure 3(b), undergoing the two-step process elaborated in section 3 of the Supplementary Information. This transition, similar to that presented in the main text, is mediated by a supercritical pitchfork bifurcation (inset of figure 3), where the bifurcation parameter here is now the body aspect ratio a_z/a in place of δ_{AC}/a .

2.2.2. Phase VI \rightarrow VII

We further demonstrate the Phase VI \rightarrow VII transition at constant $\delta_{AC}/a = 0.21$, illustrating it via geometric variation alone. We start by considering a spheroid of aspect ratio $a_z/a = 0.3$ as shown in figure 4(a), where we encounter the characteristic outer rings oriented orthogonally to the inner ones (Phase VI). Upon decreasing δ_{AC}/a to a critical value, we can observe that the stable NSS (blue) approach the body and the stable FSS (purple) in the outer rings, ultimately passing through the FSS pairs as the outer rings “kiss” and reorient orthogonally, thus reorganizing the flow into the finite thickness layer regime of Phase VII (figure 4(b)). This transition, similar to that presented in the main text, is mediated by a higher-order elliptic reflecting umbilic bifurcation (Bosschaert & Hanßmann 2013).

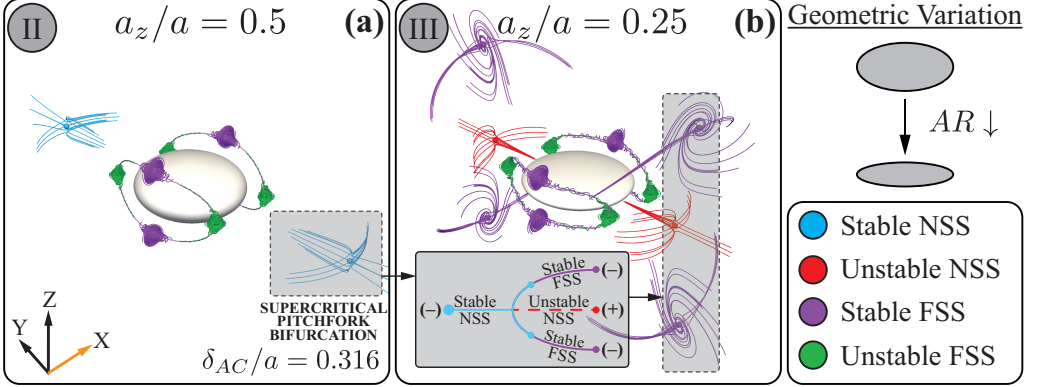


FIGURE 3. Bifurcation through curvature variation in non-axisymmetric case. We keep the flow parameter $\delta_{AC}/a = 0.316$ constant. **(a)** Streaming from spheroid with aspect ratio $a_z/a = 0.5$ illustrates a flow representative of Phase II. **(b)** Decreasing a_z/a to 0.25, while keeping δ_{AC}/a constant, triggers a supercritical pitchfork bifurcation that splits the stable NSS (blue) into an unstable NSS (red) and two stable FSS (purple). Simulation details: normalized uniform grid spacing $h/a = 0.03$.

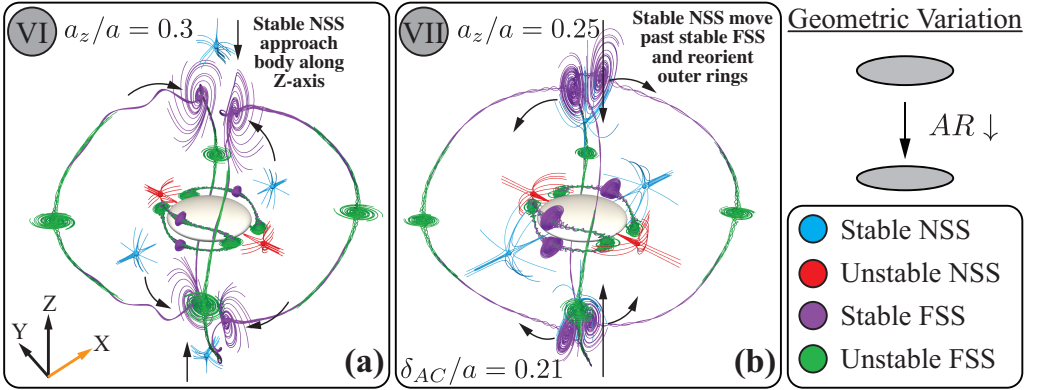


FIGURE 4. Bifurcation through curvature variation in non-axisymmetric case. We keep the flow parameter $\delta_{AC}/a = 0.21$ constant. **(a)** Streaming from spheroid with aspect ratio $a_z/a = 0.3$ illustrates a flow representative of Phase VI, where the outer rings are oriented orthogonally relative to the inner ones. **(b)** Decreasing a_z/a to 0.25, while keeping δ_{AC}/a constant, induces the reorientation of the outer rings as the stable NSS move past the adjacent stable FSS pair. Simulation details: normalized uniform grid spacing $h/a = 0.03$.

3. Two-step transition in non-axisymmetric cases

We describe here the two-step process encountered in multiple transitions observed in the main text. We start by recalling the Phase II \rightarrow III transition and describe the two-step process in detail (figure 5). As we decrease δ_{AC}/a from Phase II (figure 5(a)), the stable NSS on each side of the body first splits into an unstable NSS (red) and a pair of stable NSS (blue) through a supercritical pitchfork bifurcation, resulting in the flow structure of figure 5(b). Upon a further decrease in δ_{AC}/a , we can observe that the new pair of stable NSS (blue) moves apart from each other and away from the unstable NSS (red), and begins to develop local rotational flow, thus transitioning from stable NSS (blue) to stable FSS (purple), as illustrated in figure 5(c). It is important to highlight here that in the second step of the process (figure 5(b,c)), the stability and the number of these points are preserved across system changes (from NSS to FSS), suggesting that

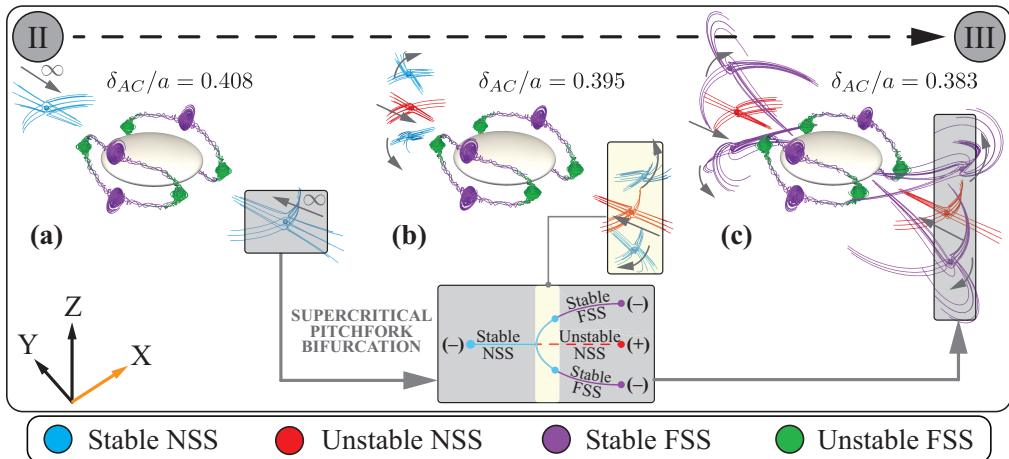


FIGURE 5. Two-step process of pitchfork bifurcation for Phase II \rightarrow III transition. Stable NSS (blue) in (a) Phase II first splits into an unstable (red) and two stable (blue) NSS, resulting in a (b) hidden phase, before ultimately transitioning to (c) Phase III when the new stable NSS change in nature into stable FSS (purple). Simulation details: normalized uniform grid spacing $h/a = 0.03$ (used throughout this section).

a bifurcation may not be the appropriate description, but rather a focus–node transition similar to Barnes & Grimshaw (1997) has occurred. We further note that this two-step process occurs in the subcritical pitchfork bifurcation of Phase IV \rightarrow V transition as well, with the stability of the involved critical points throughout the transition now opposite of those described above.

4. Identification of critical points

Here we describe the methodology employed to identify critical points in our simulations. In particular, we follow the procedure below.

(i) **Extraction of zero velocity points.** We apply a minimum filter to scan over the entire velocity field via a moving box, which isolates and outputs points that are local minima. The size of this box is a user-defined parameter, where setting it too small results in noisy outputs, while setting it too large effectively masks out existing, nearby critical points. Here we set a cubic box of size based on the minimum system characteristic length scale $\mathcal{O}(\delta_{AC}/a) \sim 0.1$. The resulting points from the filter are then further processed via a velocity threshold condition so that we eliminate points with velocity magnitudes larger than 10^{-12} . This is a value close to machine precision (we used double precision in all our calculations) and orders of magnitude smaller than the streaming velocity scale $\mathcal{O}(\epsilon^2 a \omega)$.

(ii) **Classification and observation.** We compute the eigenvalues/eigenvectors of the Jacobian associated with the velocity field at the identified critical points, and classify these points accordingly, as detailed in Section 3.2 of the main text. We further seed tracer particles in the vicinity of these points and observe that local flow patterns are indeed consistent with the previously identified critical point types.

(iii) **Validation.** We compared with previous theoretical, experimental, and numerical observations available for 2D cylinders (Parthasarathy *et al.* 2019; Bhosale *et al.* 2020) and 3D spheres (Lane 1955) and spheroids (Kotas *et al.* 2007). In all these cases, we consistently recover reported flow topologies and critical points.

We further perform the following consistency checks:

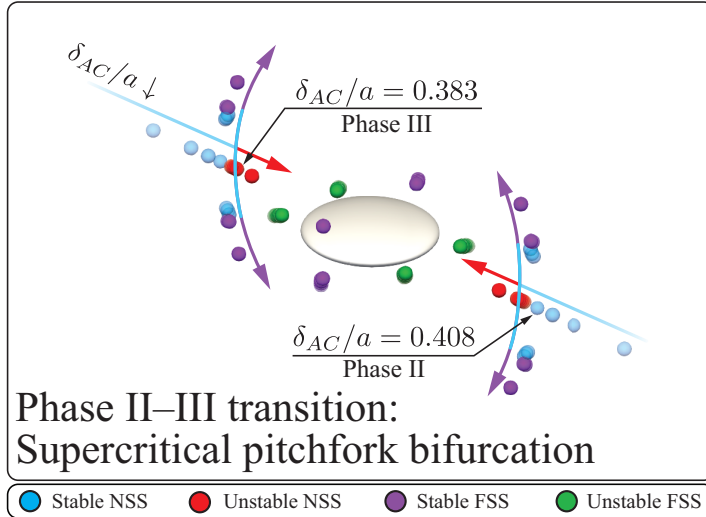


FIGURE 6. Trajectories of critical points transitioning from Phase II to III as δ_{AC}/a decreases, as indicated by increasing opacity. Values of δ_{AC}/a presented in the main text for Phase II and III are highlighted accordingly.

(i) **Simulation resolution.** We performed a set of simulations at double the mesh grid resolution of those reported in the manuscript for all the phases presented (Phase I–VII). We recovered exactly the same number and type of critical points.

(ii) **Robustness to perturbation in the bifurcation parameter.** For a given streaming flow topology, we perturb the value of δ_{AC}/a (without invoking a bifurcation) and observe that the captured critical points remain invariant. More details can be found in section 5 below.

(iii) **Symmetry cross-checks.** We further take advantage of the discrete symmetry in our problem setup and, as a sanity check, confirm that symmetry in the existence/emergence of the critical points is preserved in all instances. In other words, a critical point that exists on one side of the oscillating body must exist on the other side as a reflection along the plane of symmetry. We consistently recover such symmetry and do not observe any deviation from it in any instance.

We note here that we cannot mathematically prove the methodology above captures all the existing critical points in a general 3D flow field. However, given the protocols and consistency checks described above, we are reasonably confident that we have not missed any of the critical points for the specific scenarios presented in the paper.

5. Identification of bifurcation

In order to ensure that the bifurcations occur as indicated in the manuscript, we have investigated more δ_{AC}/a values than presented in the main text. We first identify distinct phases through a coarse δ_{AC}/a scan, and then perform additional simulations via a bisection approach to precisely pinpoint the δ_{AC}/a bifurcation value.

Here, as an example, we demonstrate the approach here for the Phase II–III supercritical pitchfork bifurcation presented in the main text. In figure 6 below, we illustrate the trajectories of the critical points as δ_{AC}/a decreases (indicated by the increasing opacity of the visualized points). The δ_{AC}/a values presented in the main text are also marked in figure 6. This approach not only allows us to accurately determine the bifurcation

parameter values, but also provides us with a large set of simulations, that we use to test the robustness of our critical point extraction methods (section 4 above). We find that critical points are consistently recovered across simulations, further reinforcing the approach presented in section 4 above.

REFERENCES

- BARNES, BELINDA & GRIMSHAW, ROGER 1997 Analytical and numerical studies of the bonhoeffer van der pol system. *The ANZIAM Journal* **38** (4), 427–453.
- BHOSALE, YASHRAJ, PARTHASARATHY, TEJASWIN & GAZZOLA, MATTIA 2020 Shape curvature effects in viscous streaming. *Journal of Fluid Mechanics* **898**, A13.
- BOSSCHAERT, MAIKEL & HANSSMANN, HEINZ 2013 Bifurcations in hamiltonian systems with a reflecting symmetry. *Qualitative Theory of Dynamical Systems* **12** (1), 67–87.
- KOTAS, CHARLOTTE W, YODA, MINAMI & ROGERS, PETER H 2007 Visualization of steady streaming near oscillating spheroids. *Experiments in fluids* **42** (1), 111–121.
- LANE, CA 1955 Acoustical streaming in the vicinity of a sphere. *The Journal of the Acoustical Society of America* **27** (6), 1082–1086.
- PARTHASARATHY, TEJASWIN, CHAN, FAN KIAT & GAZZOLA, MATTIA 2019 Streaming-enhanced flow-mediated transport. *Journal of Fluid Mechanics* **878**, 647–662.